Articles
doi.org/10.1002/batt.201900199

Chemistry Europe
European Chemical Societies Publishing

Special Collection

Effects of Crosslinker Concentration in Poly(Acrylic Acid)-KOH Gel Electrolyte on Performance of Zinc-Air Batteries

Thuy Nguyen Thanh Tran,[a] Michael P. Clark,[a] Hyun-Joong Chung,[a] and Douglas G. Ivey*[a]

Zinc-air batteries (ZABs) using gel polymer electrolytes suffer from low energy efficiency and poor cyclability. This issue is not only associated with the air electrode, as early failure of the battery is often due to the Zn electrode. Here, the cycle life of ZABs using alkaline poly(acrylic acid) (PAA-KOH) as the electrolyte is shown to vary by changing its crosslinking density. For ZABs using hydrogel electrolytes, understanding the failure mechanism and optimization of the hydrogel composition are key to achieving better utilization of the Zn electrode and battery rechargeability. In addition, the effects of crosslinker concentration on rheological properties, sol-gel fraction, ionic conductivity, and water retention ability of the hydrogel are discussed. PAA-KOH gels with lower crosslinking concentrations are weaker, but they have higher conductivity and better water retention, whereas gels with higher crosslinking concentrations affect the diffusion of zincate ions and facilitate passivation of the Zn electrode, resulting in early failure of the battery.

1. Introduction

In the continuing search for sustainable energy storage systems, zinc-air batteries (ZABs) stand out as promising candidates with high energy density, long shelf life when sealed, safe operation and no environmental issues.[1] Zn is also readily available; e.g., Natural Resources Canada reported in 2017 that Canada produced 344,294 tonnes of Zn, ranking it fourth among the world's producers of refined Zn.[2] Going forward, the abundance of Zn offers the potential for lower cost ZABs relative to Li-ion batteries. Until now, the most successful applications for ZABs thus far have been in the primary battery market, including portable medical and telecommunication devices.[3] The development of secondary ZABs is constrained by the performance of the air electrode which limits the round-trip efficiency and cycle life of rechargeable ZABs.[4] Considerable research has been done on bifunctional catalysts for the air electrode to lower the energy barrier for both the oxygen evolution reaction (OER) and oxygen reduction reaction (ORR) in order to improve the energy efficiency of ZABs.[5–7] Other engineering solutions including mechanically rechargeable ZABs and Zn-air flow batteries, in which the electrolyte is circulated in the cell system, have also been proposed.[8–10] These solutions may be effective for grid energy storage applications, but they add cost and complexity to the system. Furthermore, there have been several reports incorporating tri-electrode designs, where the OER and ORR catalysts are separated to improve ZAB performance.[11–17] A tri-electrode design has its drawbacks, however, since the design is more complex and the specific energy is invariably reduced by the extra mass associated with extra OER electrodes. There are also issues associated with the alkaline, aqueous electrolyte (e.g., KOH) used in ZABs, as it is prone to evaporation, carbonation and flooding.[18] Since electrolytes play a key role in the transport of active species, new electrolyte materials are needed to overcome these challenges.

To alleviate problems associated with carbonation, aqueous, near-neutral electrolytes have been proposed. ZABs with LeClanché-based electrolytes containing NH_4Cl–$ZnCl_2$ have shown good cyclability, but the strongly oxidizing characteristic of chlorine and the precipitation of unwanted salts during gradual evaporation of water still hinder the development of a robust battery.[18,19] Room temperature ionic liquids (RTILs), which are liquid-state salts under ambient condition, have been employed to address evaporation associated with aqueous electrolytes, since they are non-volatile and more thermally and electrochemically stable.[20] However, the ionic conductivity of RTILs is approximately 500 times lower than that of a standard KOH solution, which limits their application in ZABs.[21] Another type of electrolyte is gel polymer electrolytes (GPEs). GPEs employ a class of polymer known as hydrogels, which can absorb a significant amount of water without dissolving and, thus, have been utilized as base materials to hold alkaline solutions in ZABs. The major applications for using GPEs in ZABs have almost exclusively been for wearable electronic devices. It is also notable that most of the recent reports have chosen poly(vinyl alcohol) (PVA) as the gel polymer matrix. Pioneered by Fu et al.[22] and Peng et al.[23] in 2015, rechargeable, flexible and stretchable ZABs with a PVA-based alkaline electrolyte had poor cyclability and low current densities; e.g., ~100 cycles at 0.01–0.1 mA cm^{-2}. Recently, Zhou et al. reported that ZABs using PVA-KOH could last 60 cycles at 6 mA cm^{-2},[24] while Fan et al. developed ZABs (with PVA-KOH) that showed stable charge and discharge at 3 mA cm^{-2} for 36 cycles.[25] Lei et al. have

[a] T. N. T. Tran, M. P. Clark, Prof. H.-J. Chung, Prof. D. G. Ivey
Department of Chemical and Materials Engineering
Faculty of Engineering, University of Alberta
Edmonton, Alberta, T6G 1H9, Canada
E-mail: divey@ualberta.ca

Supporting information for this article is available on the WWW under https://doi.org/10.1002/batt.201900199

Special Collection An invited contribution to a Special Collection on Electrolytes for Electrochemical Energy Storage

reported the longest cycle life (80 cycles) for solid-state ZABs at a low current density of 1 mA cm^{-2}.[26] Direct comparisons are difficult to make among the various references, since tests were not done under the same operating conditions. The types of bifunctional catalysts, cycling test parameters, the concentration of the aqueous electrolyte within the polymer and the molecular weight of PVA were different.

In a previous study by some of the authors, different hydrogel matrices for KOH solutions were assessed based on mechanical strength, electrochemical and chemical stability, ionic conductivity, water uptake and battery performance.[27] Among them, poly(acrylic acid) impregnated with KOH (PAA-KOH) was the most promising candidate to replace traditional alkaline solutions. As the polymeric host material, PAA is chemically and electrochemically stable under highly alkaline environments. The conductivity of PAA-KOH remains stable at high temperatures (360 mS cm^{-1} at 65 °C) because of its high water retention.[27] In battery testing, ZABs with PAA-KOH electrolytes have the potential to outperform batteries with conventional aqueous electrolytes (e.g., 6 M KOH) by reducing interfacial and charge transfer resistance. In another study by the authors, leakage issues associated with aqueous electrolytes were prevented, allowing the battery to operate in different orientations when using PAA-KOH.[28] The optimal concentration of crosslinker (N,N′-methylenebis(acrylamide) or MBAA) was affected by the characteristics of the Ni current collector, specifically, a less porous Ni foam structure inhibits PAA-KOH penetration, while a more porous structure facilitates penetration and increases water evaporation from the PAA-KOH.[28] For a bi-electrode design, the most frequently used material to support bifunctional catalysts is a Teflon-coated carbon paper, known as a gas diffusion layer (GDL).[29–32] Unlike Ni foam, GDL combines characteristics such as porosity (to allow access to oxygen gas) and hydrophobicity (to prevent flooding of aqueous electrolytes). In spite of the numerous studies done on ZABs that employ PAA-KOH as electrolytes,[33–35] there is still a lack of systematic optimization of PAA composition.

The aim of this study is to characterize and optimize the compositions of PAA-KOH electrolytes for bi-electrode ZABs that use a conventional GDL as the support base for bifunctional catalysts. The impact of varying crosslinker concentration on gel properties, including loss and storage moduli, sol-gel fraction, ionic conductivity and water retention ability, are discussed. Attempts are made to explain the effects of crosslinking density on cycling performance of ZABs at a current density of 5 mA cm^{-2}. Changes to the Zn electrode morphology in cells using PAA-KOH electrolyte after cycling are also compared with morphology changes in aqueous electrolytes to understand the factors affecting ZAB failure.

Experimental Section

Synthesis of catalysts

All chemicals were of analytical grade (>99%) and used as received without further purification. L-ascorbic acid (L-AA) and sodium dodecyl sulfate (SDS) were obtained from Sigma-Aldrich. Manganese(II) sulfate, sodium acetate, cobalt(II) sulfate, sodium citrate and boric acid were obtained from Fisher. Iron(II) sulfate was obtained from MP. Deionized water (DIW) was used to rinse and prepare all aqueous solutions. The gas diffusion layer (GDL) (Teflon-coated porous carbon paper, Sigracet 39 BB) was obtained from the Fuel Cell Store. The GDL was divided into 5 cm^2 sections and used as the substrate for electrodeposition.

Sequentially electrodeposited MnO_x/Co–Fe on GDL was utilized as the bifunctional air electrode; MnO_x provides ORR activity, while Co–Fe provides OER activity. Details regarding fabrication and characterization of the catalysts can be found in the literature.[31] Briefly, electrodeposition of catalysts was performed at 40 °C in a two-electrode cell where GDL and Pt mesh were used as working and counter electrodes, respectively. First, anodic deposition of MnO_x was carried out at a constant current of 40 mA for 10 min in a solution containing $MnSO_4$ (0.1 M), sodium acetate (0.1 M) and SDS (100 mg L^{-1}). Samples were rinsed with de-ionized water (DIW) and then annealed at 300 °C for 30 min. Cathodic deposition of Co–Fe was then done at a constant current of 200 mA for 2 min in a solution containing $CoSO_4$ (0.15 M), $FeSO_4$ (0.05 M), sodium citrate (0.2 M), boric acid (0.2 M), L–AA (0.05 M) and SDS (400 mg L^{-1}). Samples were rinsed with DIW afterwards and then dried in air.

Synthesis of hydrogel electrolyte

PAA was used as the host polymer for the PAA-KOH gel electrolyte in this work. Acrylic acid (AA), MBAA and potassium persulfate (KPS) were obtained from Sigma-Aldrich, while potassium hydroxide (KOH) was obtained from Fisher Scientific. PAA-KOH was prepared by mixing 7.5 M KOH, 1.5 M AA, KPS thermoinitiator (0.1 mol% of AA monomers) and MBAA crosslinker (0.1, 0.3, 0.5, 0.7 or 0.9 mol% of AA monomers). The polymer electrolytes, with different crosslinking concentrations, are hereafter denoted as MBAA 0.1, MBAA 0.3, MBAA 0.5, MBAA 0.7 and MBAA 0.9, respectively. The electrolyte solutions were kept in an oven at 60 °C for 1 h to carry out polymerization and then allowed to cool overnight to room temperature.

Cell fabrication

Two designs for bi-electrode ZABs were fabricated and are shown in Figure 1. The different designs were necessary because aqueous KOH electrolyte and PAA-KOH gel electrolyte, respectively, require different device configurations. Both cells were made from a frame of acrylic sheets and the air electrode was positioned on top with a Zn electrode below. The ZAB using PAA-KOH as the electrolyte was stacked in layers (Figure 1a), while the cell built using a conventional aqueous KOH electrolyte (6 M concentration) needed the walls to be sealed to prevent leaking (Figure 1b). In addition, a hole was cut on top of the cell for electrolyte refilling purposes. The contact area between the air electrode and electrolyte, for both cells, was controlled (1 cm^2) and the total mass of Zn used was ~1 g (0.2 mm thick).

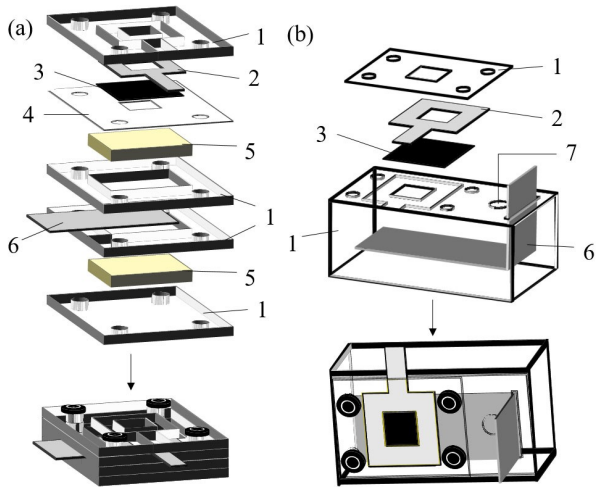

Figure 1. Homemade cell assembly for bi-electrode ZABs using a) a PAA-KOH electrolyte and b) an aqueous electrolyte. 1: Acrylic sheets, 2: current collector Ni, 3: GDL, 4: polypropylene film, 5: GPE, 6: zinc, 7: refilling hole.

Material characterization

The morphologies of the air and Zn electrodes, before and after battery cycling, were characterized using scanning electron microscopy (Zeiss EVO M10 SEM and Zeiss Sigma FESEM (field emission)), coupled with energy dispersive X-ray (EDX) spectroscopy. The amount of ZnO coverage on the Zn electrode surface was of particular interest. EDX spectra were taken from several areas of the Zn electrode. For batteries using aqueous electrolyte, the Zn electrode was cleaned with DIW to remove any residual KOH before SEM imaging, so the amount of ZnO coverage on the Zn surface was directly correlated with the amount of oxygen [Eq. (1)].

$$\%\mathrm{ZnO} = \mathrm{at}\,\%\mathrm{O} \div \mathrm{at}\,\%\mathrm{Zn} \times 100\,\% \quad (1)$$

For batteries using PAA-KOH as the electrolyte, the Zn electrode was not cleaned with DIW prior to SEM examination to prevent swelling of any PAA-KOH that may be covering portions of the Zn electrode. Thus, the amount of ZnO on the Zn electrode surface was determined after subtracting the oxygen amount from PAA-KOH and KOH, which are related to the amount of C in the polymer ($C_3H_4O_2$) and K in the KOH, respectively. The amount of ZnO was then calculated from Equation (2):

$$\%\mathrm{ZnO} = \left(\mathrm{at}\,\%\mathrm{O} - \frac{2}{3}\mathrm{at}\,\%\mathrm{C}(\mathrm{in}\ \mathrm{C_3H_4O_2}) - \mathrm{at}\,\%\mathrm{K}(\mathrm{in}\ \mathrm{KOH})\right) \div \mathrm{at}\,\%\mathrm{Zn} \times 100\,\% \quad (2)$$

where at% signifies the amounts of the elements in atomic percent.

Conductivities for PAA were measured by electrochemical impedance spectroscopy (EIS) at open circuit potential with an applied 10 mV AC potential from 100 kHz to 10 mHz using a potentiostat/galvanostat (Autolab PGSTAT302 N). Rheological properties were characterized with a rheometer (Kinexus Lab+). First, the linear viscoelastic region (LVER) was determined by an amplitude sweep from 0.1–100% strain at 1 Hz and then a frequency sweep at 1% strain was done from 0.01–10 Hz.

The masses of as-prepared PAA-KOH electrolytes (W_{gel}) with different crosslinker amounts were determined from the sum of the mass of the components. Then the samples were neutralized with 1 M HCl and rinsed with DIW. The gels were freeze-dried overnight and dried again in a vacuum oven at 45 °C to achieve a completely dried state (W_i). For sol-gel fraction analysis, the dried PAA samples were subjected to Soxhlet extraction using DIW as the solvent at 100 °C for 12 h. Extracted gels were dried again. The gel fraction was calculated from the masses of the initial dry gel (W_i) and the extracted dry gel (W_f) :[36,37]

$$\text{Sol fraction}\ (\%) = \left[\frac{W_i - W_f}{W_i}\right] \times 100$$

$$\text{Gel fraction}\ (\%) = 100 - \text{Sol fraction}$$

For evaporation tests, 3 mL of aqueous 6 M KOH and PAA-KOH with different crosslinker amounts (0.1, 0.3, 0.5, 0.7 and 0.9 mol%) were contained in separate tubes, each with an open area of 0.8 cm^2 ($d = 1$ cm). The tubes were kept under vacuum at 45 °C. The tube masses were measured at 1 h intervals over an 8 h period. The mass loss at each interval was equal to the tube mass at a particular interval minus the mass from the previous interval.

Battery testing

For rate testing, battery potential was measured using a galvanostatic method for a range of current densities, i.e., 2, 5, 10 and 20 mA cm^{-2}, for 10 min each with cut-off voltages of 0.8 V (discharge) and 2.5 V (charge). Cycling tests were also done through a galvanostatic method with 30 min per cycle using another potentiostat/galvanostat (Biologic VSP-300). The battery was discharged and charged at 5 mA cm^{-2} for 10 min and the circuit was kept open for 5 min between steps. The purpose of the battery rest period between discharging and charging was to allow the battery to stabilize and cool. Blurton et al. found that heat generation during discharge and charge is a major consideration for battery management, as it can facilitate self-discharge and water evaporation.[38] The discharge-charge efficiency was calculated by dividing the lowest discharge potential by the highest charge potential during one cycle.

2. Results and Discussion

2.1. Properties of PAA-KOH Gel Electrolytes

The states of PAA-KOH can be visibly assessed, as shown in Figure 2a. Tubes containing the various electrolytes were inverted and the flow behavior was observed. After 2 min, the MBAA 0.1 sample was the only electrolyte to flow. In order to assess the mechanical behavior of the solid hydrogels, rheological measurements were made to determine the ratio between the elastic modulus G' (reversibly stored energy; mechanical strength as a continuum) and the viscous modulus G'' (irreversibly lost energy; dissipated by viscous flow) for each PAA-KOH gel electrolyte with varying MBAA (crosslinker) concentration. Tan(δ) was used to quantify the balance between lost and stored energies, where δ is the phase angle. Conventionally, gels (solid-like state) are considered to have formed when $\tan(\delta) = G''/G'$ is less than 1, whereas $\tan(\delta)$ larger than 1 corresponds to a sol (liquid-like state). Firstly, an amplitude sweep at a frequency of 1 Hz was carried out on PAA-KOH to determine its linear viscoelastic region (LVER),

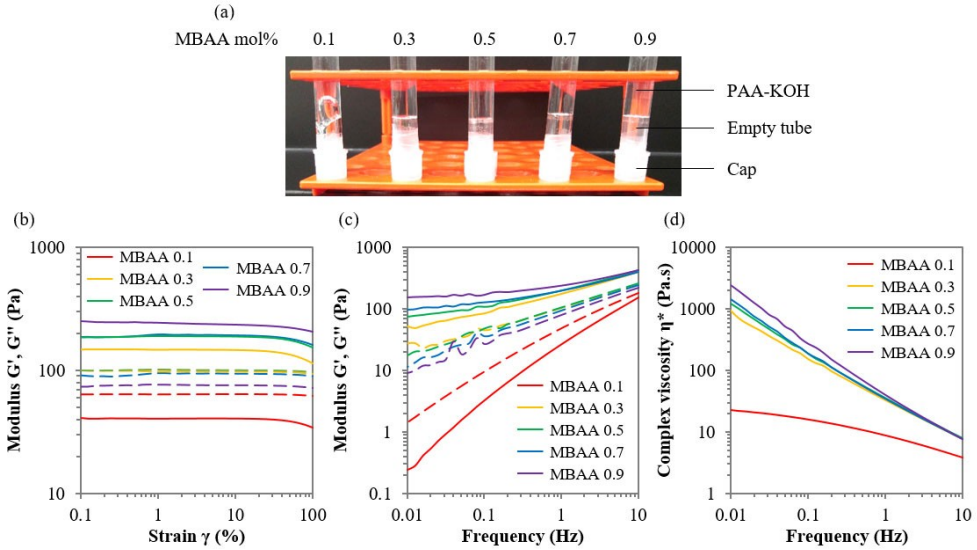

Figure 2. Rheological properties of PAA-KOH with varying crosslinking concentrations. a) Photograph showing flow behavior of various GPEs 2 min after the containers have been inverted. b) LVER region for the GPEs determined by amplitude sweeps from 0.1 to 100% strain at 1 Hz. c) G' and G''moduli as a function of frequency. d) Complex viscosity determined by a frequency sweep. In b) and c), the solid lines represent the G' modulus and the dashed lines represent the G''modulus.

where the elastic modulus remains constant over a small change in the strain (Figure 2b). PAA-KOH with 0.1 mol% MBAA has a tan(δ) value of 1.56 in the LVER. In accordance with the physical appearance of a viscous fluid (leftmost vial in Figure 2a), the crosslinker content is not sufficient to form a gel. As the MBAA concentration is increased from 0.3 to 0.9 mol%, G' values increase from 149 to 250 Pa, while G'' values decrease from 101 to 74 Pa in the LVER. All PAA-KOH samples with MBAA concentration in the range of 0.3 to 0.9 mol% can be considered as GPEs, since the tan(δ) values are below 1. Hydrogels formed using higher crosslinking agent concentrations have shorter strand lengths between crosslinks and are more physically stable.[39,40]

Secondly, a frequency sweep between 0.01 and 10 Hz was performed at 1% maximum strain, which is within the LVER of the polymers. In an ideal gel system, the tan(δ) value is nearly constant over wide frequency ranges.[41–43] As with the amplitude sweep, G' is higher than G'' for PAA-KOH containing 0.3 to 0.9 mol% MBAA over the entire frequency range, whereas G'' is higher than G' when 0.1 mol% MBAA is added (Figure 2c). A plot of complex viscosity as a function of frequency, $|\eta^*| = \sqrt{(G'/\omega)^2 + (G''/\omega)^2}$, is shown in Figure 2d, based on the data in Figure 2c. The complex viscosity is almost independent of frequency for 0.1 mol% MBAA, which means that the sample is a fluid with a non-associated structure.[43,44]

In low-molecular-weight polymer electrolytes (~2000 g/mol for poly(ethylene oxide)), ionic conduction takes place by two means.[45,46] In the first mechanism, which is known as fluctuation-driven diffusion, ion motion is mediated by segmental motion of the surrounding polymer chains. As such, conduction is determined by interactions between ions and polymers and the glass transition temperature (T_g) of the polymer. The second mechanism, vehicular diffusion, occurs by the diffusion of the whole polymer chain interconnected with ions.[47] As shown in Figure 3a, crosslinker amount does not change the total mass or volume of PAA-KOH significantly; thus the ratio between the weight of as-prepared PAA-KOH and dry PAA remains approximately constant (11.7 to 11.8). Sol-gel fraction analysis was carried out to determine the uncrosslinked fraction of AA monomers and whether or not this fraction contributes to ionic conductivity. The gel fraction of the hydrogels (i.e., fraction of AA monomer that participated in gelation) increases with increasing crosslinker content (Fig-

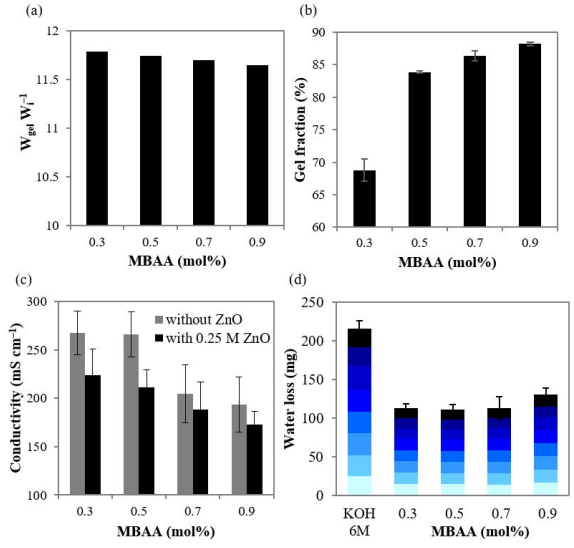

Figure 3. a) Ratio between the weight of as-prepared PAA-KOH and dry PAA. b) Gel fraction, c) ionic conductivity, and d) water loss for PAA-KOH as a function of crosslinker concentration.

ure 3b). PAA-KOH with 0.3 mol% MBAA and 0.5 mol% MBAA have the same conductivities, i.e., 270 mS cm^{-1}, even though the 0.3 mol% MBAA sample had 15% more sol fraction. With the addition of ZnO, however, the ionic conductivities showed a nearly monotonic decrease with increasing MBAA content (224, 211, 188 and 173 mS cm^{-1} for 0.3, 0.5, 0.7 and 0.9 mol% MBAA, respectively - Figure 3c). This result indicates that the actual ionic conductivity may be dependent on the interplay between the effective mesh size and the hydrodynamic radius of charge conducting ions. When ZnO particles are dispersed into an alkaline solution, zincate complexes ($Zn(OH)_4^{2-}$) are formed with a thin electric dipole layer of the solvent attached to the complex surface which influences the Brownian motion of the particles in the medium.[48] Pessine et al. reported that the "solvodynamic radii" of $Zn(OH)_4^{2-}$ calculated from the Stokes-Einstein equation had a range of values from 0.35 to 0.41 nm.[48] For hydroxide ions, Roobottom et al. reported that the "thermochemical radius" is 0.152 nm.[49] This size is comparable to the radius of $H_9O_4^-$ (OH^- ion forming hydrogen bonds with four adjacent water molecules) which was reported to vary from 0.138 to 0.16 nm.[50] Based on these references, it is hypothesized that zincate ions are large enough that their transport may be hindered by the PAA mesh at high MBAA content, leading to a lower conductivity for PAA-KOH.

Hydrogels, especially PAA, have a wide range of applications within agriculture, cosmetic and hygienic products, the pharmaceutical industry and wastewater treatment, all because of PAA's high absorbance and water retention ability.[51,52] These attributes can have a substantial impact on ZABs as well. ZABs use oxygen from the air for the ORR reaction, so water evaporation is inevitable. PAA electrolytes can reduce water loss, which was demonstrated by exposing PAA-KOH with different MBAA concentrations, as well as an aqueous KOH solution (6 M KOH), to a vacuum for 8 h at 45 °C. As shown in Figure 3d, PAA electrolytes can reduce water loss by 50% compared with aqueous KOH solutions. This is achievable due to the water states in hydrogels, which can be classified into three types: normal water/water interaction (free water), weakened water/water interaction (weakly bound water to the polymer) and extremely weakened water/water bonding (strongly bound water to the polymer). The structure of free water is similar to that of bulk water and its interaction with polymer chains is negligible. On the other hand, functional groups in the hydrogels can capture nearby water molecules through hydrogen bonding or other strong interactions, leading to the formation of strongly bound water. Weakly bound water is due to second-order interaction between the nearly-free water molecules and the strongly bound water molecules.[53,54] It was previously reported that even when free water is expelled from a hydrogel network, bound water still remains.[55] Water retention is similar for PAA-KOH with 0.3, 0.5 and 0.7 mol% MBAA (112.7, 111.6 and 113.3 mg of water loss, respectively). However, there is a more marked decrease for 0.9 mol% MBAA (130.2 mg of water loss). A higher crosslinking density may create a denser network which affects the interaction between carboxyl functional groups of PAA with surrounding water molecules. The polymer structure then collapses, so that the network voids available for retaining water are minimized and water retention is decreased.[56]

2.2. Performance of Zinc-Air Batteries

ZABs were fabricated by sandwiching the electrolyte between Zn metal sheet and GDL coated with the ORR/OER catalyst (MnO_x/Co–Fe). The deposition of MnO_x/Co–Fe on the GDL generated several cracks on the surface (Figure 4a). As such, pathways for diffusion of oxygen into the ORR reaction zone still existed. The thickness of the MnO_x/Co–Fe layer on the GDL was ~7–9 μm, which was confirmed through cross-sectional SEM imaging of the catalysts on GDL (Figure S1a). According to the EDX line scans (Figure S1b), the catalyst layer is Fe/Co-rich on the surface with larger amounts of Mn in the subsurface region. Rate tests at several current densities for batteries using PAA-KOH as the electrolyte, with different MBAA concentrations, are shown in Figure 4b. The MBAA amount has minimal influence on the discharge potential, but significantly affects the charge potential. Specifically, the charge potential reached a limiting value of 2.5 V at 20 mA cm^{-2} for PAA-KOH with 0.9 mol% MBAA. These results are similar to previous work done by the authors using PAA-KOH electrolyte in a tri-electrode battery design.[28]

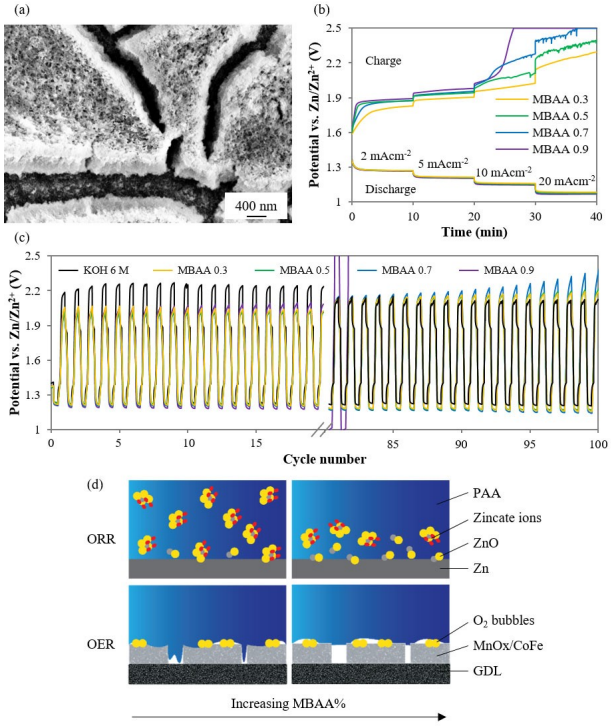

Figure 4. a) FESEM image of MnOx/Co–Fe on GDL. Evaluation of ZABs using PAA-KOH with various MBAA concentrations: b) rate discharge-charge curves and (c) cycling performance at 5 mA cm^{-2}. (d) Schematic illustration of the effects of crosslinking density on discharge and charge of a ZAB. White regions in the schematic represent cracks in the catalyst layer or gaps at the catalyst/electrolyte interface.

Battery cycling tests were done at a current density of 5 mA cm^{-2} for the four types of PAA-KOH electrolytes and for aqueous KOH. Initially, ZABs using PAA-KOH as the electrolyte exhibit better performance than the battery with aqueous 6 M KOH as the electrolyte. Discharge potentials for the ZAB cell using 6 M KOH are about the same as the cells using PAA-KOH; however, the charge potential for the cell with the aqueous electrolyte is significantly larger (about 150 mV). The discharge-charge efficiencies, which were calculated from the second cycle of the discharge-charge profiles (Figure 4c), are ~60% for ZABs using PAA-KOH and only ~55% for the ZAB using 6 M KOH aqueous electrolyte. With GPEs, zincate ions do not travel very far from the Zn surface, so Zn can be redeposited more easily resulting in a lower charge voltage. For aqueous alkaline electrolytes, to facilitate OER and reduce the likelihood of the hydrogen evolution reaction (HER), many investigators pre-saturate the electrolyte with zincate ions by dissolving ZnO powder.[57–61] The hydrogel electrolytes, as expected from our previous work, also had better performance because of improved physical contact with the air electrode which reduced both interfacial and charge transfer resistance. The hydrophobic nature of the air electrode, on the other hand, hindered contact with the aqueous electrolyte.[27]

The efficiency of the ZAB using the aqueous electrolyte gradually improved during cycling to approach the performance of the batteries with PAA-KOH (containing 0.3 to 0.5 mol% MBAA). After 80 cycles, the ZAB with the aqueous electrolyte had better efficiency; the efficiency reached 57% at the 100th cycle. The improvement in efficiency can be attributed to partial GDL degradation during OER which increased the wettability of GDL. After 100 cycles, ZABs using 0.3 or 0.5 mol% MBAA (as the electrolyte) had similar efficiencies of 53%, while the efficiency for 0.7 mol% MBAA was reduced to 48%. The ZAB with 0.3 mol% MBAA managed ~120 cycles (Figure S2), while that with 0.9 mol% MBAA only managed 80 cycles before failure. SEM images of the Zn electrode after cycling in ZAB with 0.3 mol% MBAA are shown in Figure S2 and no dendrites were found on the Zn surface.

The general mechanisms associated with the cycling behavior of ZAB using PAA-KOH with varying MBAA content as the electrolyte are illustrated in Figure 4d. During the discharge process, zincate ions diffuse into PAA-KOH. The depth of diffusion is larger for PAA-KOH with low crosslinker concentration (Figure 4d, top left) compared with PAA-KOH with high crosslinker concentration (Figure 4d, top right). For the latter case, a ZnO layer forms at the Zn/PAA-KOH interface. During cycling, the ZAB cell increases in volume, which is caused by i) the density difference between metallic Zn and the discharge product ZnO on the Zn electrode[57] and ii) by oxygen bubble accumulation during OER.[62] PAA-KOH with a low crosslinking density is soft so that the polymer network can accommodate the change in volume, i.e., the polymer can squeeze between cracks in the catalyst layer (Figure 4d, bottom left). PAA-KOH with a higher crosslinking density is stiffer and, as such, PAA-KOH may lose contact with the air electrode due to oxygen bubble accumulation (Figure 4d, bottom right). With repeated charging cycles, a layer of oxygen gas accumulates in the vicinity of the air electrode, which increases interfacial resistance, reduces the charging efficiency and even damages the battery.[62,63] Therefore, removal of the bubbles must be effectively controlled. As shown in Figure S3, adhesion between the GDL and PAA-KOH is drastically reduced when the MBAA content in PAA is increased from 0.3 mol% to 0.9 mol%. Values of adhesion strength are also shown in Table S1. A less sticky electrolyte will likely provide spaces for bubble coalescence and escape from the electrode surface; however, highly cross-linked structures will resist ion transport, which explains the similar performance for PAA-KOH with 0.3 mol% MBAA and 0.5 mol% MBAA. Even in the aqueous electrolyte, oxygen bubbles produced during the OER process can easily adhere to the charging electrode and may be stable for many hours or even days creating a significant energy barrier.[64,65] The cell potential, surface tension of the electrolyte, the properties of electrode material and bubble interaction with the electrode can influence bubble behavior.[65,66]

Cycling tests were carried out in 6 M KOH electrolytes (aqueous) with horizontal and tilted positions (Figure S4). Photographs of the cell in the tilted configuration (~15° to the horizontal) are shown in Figure S5. Overall the efficiencies are similar; however, the discharge voltage for horizontal cell is unstable and depends on oxygen bubble escape. Bubble accumulation results in a decrease in discharge potential, which recovers when the bubbles escape (Figure S4b). A brown deposit has collected at the bottom of the cell, due to loss of catalyst from the GDL (Figure S5b). In addition, the top view of the battery shows signs of electrolyte flooding (Figure S5c). Even though the battery efficiency increased during cycling for the ZAB with the aqueous electrolyte, battery integrity was compromised. Thus, ZABs using PAA-KOH are a more promising candidate for portable applications, since the hydrogel electrolyte has the benefits of being solid-state while still possessing high ionic conductivity which ensures battery integrity. Further study is needed to optimize PAA-KOH composition and battery design.

2.3. Post-Testing Analysis of the Zn Electrode

With advancements in catalysts and battery designs to assist with air electrode issues, the cycle life of rechargeable ZABs can be limited by changes in the Zn electrode related to dendrite formation, undesired relocation and passivation.[67] During recharging, Zn is redeposited onto the Zn surface from zincate ions in the electrolyte. The redeposited Zn can take the form of mossy, layer-like, boulder-like and dendritic shapes. Among these, dendrites are needle-like in nature and grow axially, which can either cause internal short circuits or detachment of Zn from the electrode, resulting in reduction of the battery capacity.[68] Moshtev et al. report that overpotential is a critical variable in dendrite formation and developed an equation to predict the time for the appearance of dendrites.[69] However, Ito et al. showed that current density ratio (effective current density over limiting current density) determines Zn morphology.[70] There are many other factors affecting dendrite

formation, including the substrate material, methods of surface preparation, electrode porosity, temperature, electrolyte composition and flow rate.[70,71] As such, a universal model governing morphology of the Zn deposit does not exist. Generally, Zn deposits tend to be mossy or spongy at low current densities, layer-like at intermediate current densities and boulder-like or dendritic at high current densities.[29] In this study, the Zn electrode was initially a flat sheet, but its morphology after cycling in the aqueous electrolyte (6 M KOH) became uneven with crystalline, hexagonal structures of Zn deposited on top of one another (Figure 5a). This morphology occurs because Zn is dissolved in the electrolyte during discharge and then re-deposited at different locations during charge. For highly porous Zn electrodes with large surface areas, the modification in morphology during cycling can result in shape change and densification of the Zn electrode, leading to the loss of utilization rate, discharge capacity and energy density of ZABs.[72]

When PAA-KOH is used as the electrolyte, Zn surface features are reduced, in part because different deposits form (Figure 5b–e). Huang et al. reported that electrostatic interaction between the negatively charged acrylate groups along the PAA-KOH chains and positively charged Zn ions formed during the discharge process produces a quasi-solid electrolyte interface between the electrolyte and Zn electrode.[73] This interaction can help retain Zn^{2+}, which is beneficial in preventing dendrite formation; however, it can also result in premature supersaturation of zincate ions and formation of ZnO. Shape change on the Zn surface is also reduced with increasing MBAA content in the electrolyte, since the presence of a stiffer solid-state electrolyte generates a larger compressive stress field around any dendritic protrusions thereby restricting their growth.[74]

Although the PAA-KOH electrolyte can restrict dendrite formation, densification and shape change of the Zn electrode, ZAB cyclability is reduced with increasing crosslinker concentration. As mentioned in Section 2.1, diffusion of zincate ions dominates when the polymer mesh size is reduced. Zincate ions can accumulate at the Zn surface leading to formation of a ZnO insulating layer which terminates the discharge process and inhibits the reverse conversion to metallic Zn, limiting battery capacity and rechargeability.[68,75] EDX analysis of the Zn electrode surface was done after cycling batteries operating with aqueous and polymer electrolytes (Figure S6). Semi-quantitative data was obtained and the results are summarized in Table 1. The Zn electrode was not passivated in the aqueous solution, but the amount of ZnO coverage on the surface of the Zn electrode increased from about 67% to 100% for ZABs using PAA-KOH with 0.3 mol% and 0.9 mol% MBAA, respectively, indicating that passivation is a major cause for failure of ZABs with polymer electrolytes during cycling.

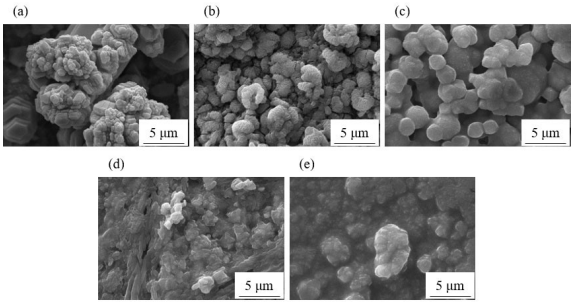

Figure 5. Morphology of Zn electrode from ZABs after cycling tests at 5 mA cm^{-2} using a) aqueous electrolyte (6 M KOH), b–e) PAA-KOH with 0.3, 0.5 0.7, and 0.9 mol% MBAA, respectively.

Table 1. EDX analysis of Zn surface after cycling test at 5 mA cm^{-2}

	C [at%]	*K [at%]*	*O [at%]*	*Zn [at%]*	*ZnO [%]*
6 M KOH	33.9	0	0	66.1	**0**
MBAA 0.3	39.2	7	41.4	12.4	**67**
MBAA 0.9	37.8	10.6	43.7	7.9	**100**

3. Conclusions

Poly(acrylic acid) impregnated with potassium hydroxide (PAA-KOH) using various crosslinker (N,N′-methylenebis(acrylamide) or MBAA) concentrations was synthesized for use as a gel polymer electrolyte for Zn-air batteries (ZABs). The effects of crosslinking density on rheological properties, sol-gel fraction, conductivities and water retention abilities of PAA-KOH were evaluated. A low concentration of MBAA (0.3–0.5 mol%) was sufficient to fabricate an effective hydrogel electrolyte; higher crosslinking densities result in lower ionic conductivity and higher water evaporation rates. ZABs using a bifunctional air electrode, consisting of a gas diffusion layer (GDL) support with a MnO_x/Co–Fe catalyst layer and PAA-KOH with 0.3 mol% or 0.5 mol% MBAA as the electrolyte, had better initial efficiencies than batteries with aqueous electrolytes (60% vs. 55%) and were relatively stable for at least 100 cycles (53% efficiency). Failure analysis of the Zn electrode after cycling shows that a higher crosslinker content in PAA-KOH can help reduce dendrite formation and densification, but facilitates passivation of the Zn surface.

Acknowledgements

This work was supported by Future Energy Systems (FES T06 P03). The authors are grateful to Rosmi Abraham for valuable discussions and Xiaoli Tan for access to the rheometer.

Keywords: N,N′-methylenebis(acrylamide) · gel polymer electrolyte · zinc-air battery · passivation

[1] S. F. Bender, J. W. Cretzmeyer, T. F. Reise, in *Handbook of Batteries, 3rd Edition*, D. Linden, T. B. Reddy, Editors. **2002**, McGraw-Hill: New York.
[2] *Zinc facts.* 2019; Available from: https://www.nrcan.gc.ca/our-natural-resources/minerals-mining/minerals-metals-facts/zinc-facts/20534.
[3] S. B. Sherman, Z. P. Cano, M. Fowler, Z. Chen, *AIMS Energy* **2018**, *6*, 121–145..

[4] Z. Wang, J. Ang, J. Liu, X. Y. D. Ma, J. Kong, Y. Zhang, T. Yan, X. Lu, *Appl. Catal. B* **2019**, *118344*..
[5] Z. Huang, X. Qin, G. Li, W. Yao, J. Liu, N. Wang, K. Ithisuphalap, G. Wu, M. Shao, Z. Shi, *ACS Appl. Energy Mater.* **2019**, *2* 4428–4438..
[6] J. Sun, H. Yin, P. Liu, Y. Wang, X. Yao, Z. Tang, H. Zhao, *Chem. Sci.* **2016**, *7* 5640–5646..
[7] K. Sakaushi, T.-P. Fellinger, M. Antonietti, *ChemSusChem* **2015**, *8*, 1156–1160..
[8] B. Pichler, B. S. Berner, N. Rauch, C. Zelger, H.-J. Pauling, B. Gollas, V. Hacker, *J. Appl. Electrochem.* **2018**, *48*, 1043–1056.
[9] P. Pei, Z. Ma, K. Wang, X. Wang, M. Song, H. Xu, *J. Power Sources* **2014**, *249*, 13–20.
[10] A. L. Zhu, D. P. Wilkinson, X. Zhang, Y. Xing, A. G. Rozhin, S. A. Kulinich, *J. Energy Storage* **2016**, *8*, 35–50.
[11] J. Zhang, Z. Zhao, Z. Xia, L. Dai, *Nat. Nanotechnol.* **2015**, *10*, 444.
[12] Y. Li, M. Gong, Y. Liang, J. Feng, J.-E. Kim, H. Wang, G. Hong, B. Zhang, H. Dai, *Nat. Commun.* **2013**, *4*, 1805.
[13] G. Toussaint, P. Stevens, L. Akrour, R. Rouget, F. Fourgeot, *ECS Trans.* **2010**, *28*, 25–34.
[14] W. Hong, H. Li, B. Wang, *Int. J. Electrochem. Sci.* **2016**, *11*, 3843–3851.
[15] G.-P. Kim, H.-H. Sun, A. Manthiram, *Nano Energy* **2016**, *30*, 130–137.
[16] Z. Yan, E. Wang, J. Gao, J. Yang, C. Wu, L. Jiang, M. Zhu, G. Sun, *ChemElectroChem* **2017**, *4*, 2190–2195.
[17] M. Xiong, M. P. Clark, M. Labbe, D. G. Ivey, *J. Power Sources* **2018**, *393*, 108–118.
[18] S. Clark, A. R. Mainar, E. Iruin, L. C. Colmenares, J. A. Blázquez, J. R. Tolchard, A. Latz, B. Horstmann, *J. Mater. Chem. A* **2019**, *7*, 11387–11399.
[19] S. Clark, A. Latz, B. Horstmann, *ChemSusChem* **2017**, *10*, 4735–4747.
[20] M.-J. Deng, J.-M. Chen, K.-T. Lu, C.-C. Wang, J.-F. Lee, J.-K. Chang, *RSC Adv.* **2012**, *2*, 9383–9386.
[21] D. Schröder, in *Analysis of Reaction and Transport Processes in Zinc Air Batteries.* Springer Fachmedien Wiesbaden, **2016**, 1–16.
[22] J. Fu, D. U. Lee, F. M. Hassan, L. Yang, Z. Bai, M. G. Park, Z. Chen, *Adv. Mater.* **2015**, *27*, 5617–22.
[23] Y. Xu, Y. Zhang, Z. Guo, J. Ren, Y. Wang, H. Peng, *Angew. Chem. Int. Ed. Engl.* **2015**, *54*, 15390–4.
[24] T. Zhou, W. Xu, N. Zhang, Z. Du, C. Zhong, W. Yan, H. Ju, W. Chu, H. Jiang, C. Wu, Y. Xie, *Adv. Mater.* **2019**, *31*, 1807468.
[25] X. Fan, J. Liu, J. Ding, Y. Deng, X. Han, W. Hu, C. Zhong, *Front. Chem.* **2019**, *7*.
[26] H. Lei, Z. Wang, F. Yang, X. Huang, J. Liu, Y. Liang, J. Xie, M. S. Javed, X. Lu, S. Tan, W. Mai, *Nano Energy* **2019**, *104293*.
[27] T. N. T. Tran, H.-J. Chung, D. G. Ivey, *Electrochim. Acta* **2019**, *327*, 135021.
[28] T. N. T. Tran, M. Xiong, M. P. Clark, H. J. Chung, D. G. Ivey, *Electrochim. Acta.* **2020**.
[29] P. Pei, K. Wang, Z. Ma, *Appl. Energy* **2014**, *128*, 315–324.
[30] L. Li, S. Liu, A. Manthiram, *Nano Energy* **2015**, *12*, 852–860.
[31] M. Xiong, D. G. Ivey, *J. Electrochem. Soc.* **2017**, *164*, A1012–A1021.
[32] M. Xiong, D. G. Ivey, *Electrochim. Acta* **2018**, *260*, 872–881.
[33] C. Guan, A. Sumboja, H. Wu, W. Ren, X. Liu, H. Zhang, Z. Liu, C. Cheng, S. J. Pennycook, J. Wang, *Adv. Mater.* **2017**, *29*, 1704117.
[34] W. Zang, A. Sumboja, Y. Ma, H. Zhang, Y. Wu, S. Wu, H. Wu, Z. Liu, C. Guan, J. Wang, S. J. Pennycook, *ACS Catal.* **2018**, *8*, 8961–8969.
[35] C. Guan, A. Sumboja, W. Zang, Y. Qian, H. Zhang, X. Liu, Z. Liu, D. Zhao, S. J. Pennycook, J. Wang, *Energy Storage Mater.* **2019**, *16*, 243–250.
[36] S. Shah, N. M. Ranjha, Z. Javaid, *Iran. Polym. J.* **2013**, *22*, 811–820.
[37] S. M. H. Bukhari, S. Khan, M. Rehanullah, N. M. Ranjha, *Int. J. Polym. Sci.* **2015**, *2015*, 15.
[38] K. F. Blurton, A. F. Sammells, *J. Power Sources* **1979**, *4*, 263–279.
[39] S. Ganguly, S. Mondal, P. Das, P. Bhawal, P. P. Maity, S. Ghosh, S. Dhara, N. C. Das, *Int. J. Biol. Macromol.* **2018**, *111*, 983–998.
[40] S. Bashir, Y. Y. Teo, S. Ramesh, K. Ramesh, *Polymer* **2018**, *147*, 108–120.
[41] M. J. Moura, M. M. Figueiredo, M. H. Gil, *Biomacromolecules* **2007**, *8*, 3823–3829.
[42] X. Liu, M. Chang, B. He, L. Meng, X. Wang, R. Sun, J. Ren, F. Kong, *J. Colloid Interface Sci.* **2019**, *538*, 507–518.
[43] L.-Y. Xia, X. Zhang, M. Cao, Z. Chen, F.-G. Wu, *Biomacromolecules* **2017**, *18*, 3073–3081.
[44] O. Arnolds, H. Buggisch, D. Sachsenheimer, N. Willenbacher, *Rheol. Acta* **2010**, *49*, 1207–1217.
[45] S. D. Druger, A. Nitzan, M. A. Ratner, *J. Chem. Phys.* **1983**, *79*, 3133–3142.
[46] A. Nitzan, M. A. Ratner, *J. Phys. Chem.* **1994**, *98*, 1765–1775.
[47] A. A. Teran, M. H. Tang, S. A. Mullin, N. P. Balsara, *Solid State Ionics* **2011**, *203*, 18–21.
[48] E. Pessine, S. Agostinho, H. Chagas, *Can. J. Chem.* **2011**, *64*, 523–527.
[49] H. K. Roobottom, H. D. B. Jenkins, J. Passmore, L. Glasser, *J. Chem. Educ.* **1999**, *76*, 1570.
[50] A. Botti, F. Bruni, S. Imberti, M. A. Ricci, A. K. Soper, *J. Mol. Liq.* **2005**, *117*, 81–84.
[51] J. Xie, X. Liu, J. Liang, *J. Appl. Polym. Sci.* **2007**, *106*, 1606–1613.
[52] Q. Lv, M. Wu, Y. Shen, *Colloids Surf. A* **2019**, *583*, 123972.
[53] K. Kudo, J. Ishida, G. Syuu, Y. Sekine, T. Ikeda-Fukazawa, *J. Chem. Phys.* **2014**, *140*, 044909.
[54] X. Zhou, F. Zhao, Y. Guo, B. Rosenberger, G. Yu, *Sci. Adv.* **2019**, *5*, eaaw5484.
[55] N. Wang, G. Ru, L. Wang, J. Feng, *Langmuir* **2009**, *25*, 5898–5902.
[56] W. B. Wang, A. Q. Wang, *Adv. Mater. Res.* **2010**, *96*, 177–182.
[57] S. Müller, F. Holzer, O. Haas, *J. Appl. Electrochem.* **1998**, *28*, 895–898.
[58] P. Bonnick, J. R. Dahn, *J. Electrochem. Soc.* **2012**, *159*, A981-A989.
[59] S. Wang, Z. Yang, L. Zeng, *J. Electrochem. Soc.* **2009**, *156*, A18-A21.
[60] J. Huang, Z. Yang, R. Wang, Z. Zhang, Z. Feng, X. Xie, *J. Mater. Chem. A* **2015**, *3*, 7429–7436.
[61] J. Yu, H. Yang, X. Ai, X. Zhu, *J. Power Sources* **2001**, *103*, 93–97.
[62] K. Wang, P. Pei, Z. Ma, H. Chen, H. Xu, D. Chen, H. Xing, *J. Power Sources* **2015**, *296*, 40–45.
[63] C. A. C. Sequeira, D. M. F. Santos, B. Šljukić, L. Amaral, *Braz. J. Phys.* **2013**, *43*, 199–208.
[64] J. H. Weijs, D. Lohse, *Phys. Rev. Lett.* **2013**, *110*, 054501.
[65] D. Zhang, K. Zeng, *Ind. Eng. Chem. Res.* **2012**. 51, 13825–13832.
[66] C. Meng, B. Wang, Z. Gao, Z. Liu, Q. Zhang, J. Zhai, *Sci. Rep.* **2017**, *7*, 41825.
[67] J. Fu, R. Liang, G. Liu, A. Yu, Z. Bai, L. Yang, Z. Chen, *Adv. Mater.* **2019**,31, 1805230.
[68] Z. Zhao, X. Fan, J. Ding, W. Hu, C. Zhong, J. Lu, *ACS Energy Lett.* **2019**, *4*, 2259–2270.
[69] R. V. Moshtev, P. Zlatilova, *J. Appl. Electrochem.* **1978**, *8*, 213–222.
[70] Y. Ito, X. Wei, D. Desai, D. Steingart, S. Banerjee, *J. Power Sources* **2012**, *211*, 119–128.
[71] R. Y. Wang, D. W. Kirk, G. X. Zhang, *J. Electrochem. Soc.* **2006**, *153*, C357-C364.
[72] J. Fu, Z. P. Cano, M. G. Park, A. Yu, M. Fowler, Z. Chen, *Adv. Mater.* **2017**, *29*, 1604685.
[73] Y. Huang, Z. Li, Z. Pei, Z. Liu, H. Li, M. Zhu, J. Fan, Q. Dai, M. Zhang, L. Dai, C. Zhi, *Adv. Energy Mater.* **2018**, *8*, 1802288.
[74] P. Barai, K. Higa, V. Srinivasan, *Phys. Chem. Chem. Phys.* **2017**, *19*, 20493–20505.
[75] Y. Wu, Y. Zhang, Y. Ma, J. D. Howe, H. Yang, P. Chen, S. Aluri, N. Liu, *Adv. Energy Mater.* **2018**, *8*, 1802470.

Manuscript received: December 3, 2019
Revised manuscript received: February 8, 2020
Accepted manuscript online: February 17, 2020
Version of record online: March 5, 2020